ADVANCED FUNCTIONAL MATERIALS
www.afm-journal.de

A Timely Synthetic Tailoring of Biaxially Extended Thienylenevinylene-Like Polymers for Systematic Investigation on Field-Effect Transistors

Dohyuk Yoo, Benjamin Nketia-Yawson, Seok-Ju Kang, Hyungju Ahn, Tae Joo Shin, Yong-Young Noh, and Changduk Yang**

Considering there is growing interest in the superior charge transport in the (*E*)-2-(2-(thiophen-2-yl)-vinyl)thiophene (TVT)-based polymer family, an essential step forward is to provide a deep and comprehensive understanding of the structure–property relationships with their polymer analogs. Herein, a carefully chosen set of DPP-TVT-n polymers are reported here, involving TVT and diketopyrrolopyrrole (DPP) units that are constructed in combination with varying thiophene content in the repeat units, where n is the number of thiophene spacer units. Their OFET characteristics demonstrate ambipolar behavior; in particular, with DPP-TVT-0 a nearly balanced hole and electron transport are observed. Interestingly, the majority of the charge-transport properties changed from ambipolar to *p*-type dominant, together with the enhanced hole mobilities, as the electron-donating thiophene spacers are introduced. Although both the lamellar *d*-spacings and π-stacking distances of DPP-TVT-n decreased with as the number of thiophene spacers increased, DPP-TVT-1 clearly shows the highest hole mobility (up to 2.96 $cm^2 V^{-1} s^{-1}$) owing to the unique structural conformations derived from its smaller paracrystalline distortion parameter and narrower plane distribution relative to the others. These in-depth studies should uncover the underlying structure–property relationships in a relevant class of TVT-like semiconductors, shedding light on the future design of top-performing semiconducting polymers.

1. Introduction

Recently, impressive progress has been made in the field of the charge carrier mobilities of organic field-effect transistors (OFETs) with solution-processable semiconducting polymers as a result of combined efforts in developing novel materials, optimizing microstructures of semiconducting film, achieving two-dimensional long-range order, and understanding charge transport physics.[1] In order to achieve high mobilities with these polymer semiconductors, new design motifs have been introduced in recent years in the form of the frameworks of maximizing intra- and inter-molecular charge transport by high co-planarity, favorable orientation of polymer chain, and strong intermolecular interactions between the neighboring molecules.[2] In line with this consideration, diketopyrrolopyrrole (DPP) has been suggested as a promising building block for constructing high-performance semiconducting polymers owing to its tight π–π spacing and long-range order induced by the high co-planarity and cross-axis dipole.[1k,3] Another appealing strategy to promote a structurally strong inter-chain aggregates is to utilize alternating electron-donating (D) and electron-accepting (A) blocks in the polymer backbones, utilizing the attractive forces between the D and A units in the neighborhood molecules.

Consequently, a current central design principle for developing top-performing semiconducting polymers in OFETs is utilizing a class of D–A polymers based on DPP. In the last 5 years, the number of publications concerning DPP-based polymers has increased 30-fold and is expected to rise further, shedding light on the outstanding charge-transport efficacy.[4] Alongside the above examples, a notable molecular set-up has recently been described by Liu et al., (*E*)-2-(2-(thiophen-2-yl)-vinyl)thiophene (TVT)-containing DPP polymers (previously called PDVTs), which has been verified as producing one of the highest mobilities observed to date for polymer semiconductors. In this method, incorporating a vinylene linkage adjacent to two thiophene rings led to an increase in the degree of co-planarity and π-conjugation along the polymer backbone through the reduced steric hindrance, thereby effectively enhancing charge transport. Following on from this, a variety of TVT-based structural derivatives, such as a naphthalenediimide (NDI)-based polymer with TVT units and selenienylene

D. H. Yoo, Prof. C. Yang
Department of Energy Engineering
School of Energy and Chemical Engineering
Low Dimensional Carbon Materials Center
Ulsan National Institute of Science and Technology (UNIST)
Ulsan 689–798, South Korea
E-mail: yang@unist.ac.kr
B. Nketia-Yawson, Dr. S.-J. Kang, Prof. Y.-Y. Noh
Department of Energy and Materials Engineering
Dongguk University
26 Pil-dong, 3 ga, Jung-gu, Seoul 100–715, South Korea
E-mail: yynoh@dongguk.edu
Dr. H. Ahn, Dr. T. J. Shin
Pohang Accelerator Laboratory
Pohang University of Science and Technology
Pohang, Kyungbuk 790–784, South Korea

DOI: 10.1002/adfm.201403527

vinylene analogues of PDVTs have been developed successfully with reasonably high mobility.[5] This indicates that TVT is one of the most promising blocks for outperforming semiconducting polymers; however, it has not been investigated systematically for the biaxially extended TVT-like polymers so far.

Therefore, with the aim of widening the understanding of TVT-like polymers, the goals in this work focus on to the effects on the intrinsic properties—including energetics, morphology, molecular packing, and charge transport—of altering the thiophene to vinylene ratio in the DPP-TVT-based polymer family. In order to achieve this goal, three DPP-TVT-n polymers, where n is the number of thiophene spacer units between DPP and TVT blocks in the repeat unit, were synthesized and characterized, and the results were discussed in terms of establishing structure–property correlations. Notably, it was discovered that structural stacking-type conformations of polymers, such as degrees of paracrystalline and (*h00*) plane distribution, rather than densely packed organization, play a dramatic role in facilitating charge transport.

2. Results and Discussion

2.1. Synthesis and Characterization

Based on published procedures, dithienyl-substituted DPP 1 was obtained by through the reaction of 2-thienylnitrile with diisopropyl succinate, followed by the installation of side-chins via alkylation.[6] Bromination of 1 using either one or two equivalents of *N*-bromosuccinimide (NBS) led to the generation of compounds 2 and 3, which were subsequently subjected to Stille coupling with either 2-trimethylstannylthiophene or 5-trimethylstannyl-2,2′-bithiophene to produce the corresponding DPP skeletons (4 and 5) with dissymmetric changes in the appended neighboring thiophene content. Both units were readily converted into dibrominated monomers 6 and 7 under treatment with NBS, respectively (**Scheme 1**a). The dibrominated monomers 3, 6, or 7 were copolymerized with *trans*-1,2-bis(tributylstannyl)ethylene via Stille-coupling polymerization to yield the target DPP-TVT-n polymers, respectively. The polymers are depicted in Scheme 1b. All polymers were purified using multiple Soxhlet extraction followed by dissolution-precipitation. The average molecular weights (M_n) of the three polymers were in the range 23.5–49.2 kDa with polydispersity indices (PDI) of 1.9–2.9, as determined using gel permeation chromatography with THF as the eluent (**Table 1**). All polymers were found to have satisfactory M_n values; the rather moderate M_n found for DPP-TVT-2 can be attributed to its reduced solubility resulting from the increased thiophene content in the backbone.

2.2. Optical and Electrochemical Properties as well as Theoretical Calculations

Figure 1 is a plot of the optical absorption spectra of DPP-TVT-0, DPP-TVT-1, and DPP-TVT-2 in solution (a) and in the solid state (b). Each polymer presents two absorption bands; the high-energy band (350–470 nm) is assigned to excited states more localized on the thiophene units and defined as the π–π^* transition, while the low-energy broad band (530–1100 nm) is assigned to excited states with a prevalent highest occupied molecular orbital (HOMO)–lowest unoccupied molecular orbital (LUMO) contribution, and is classified as intra-molecular charge transfer states (ICT). Passing from solution to thin film, there is only slight difference in the absorption maxima of all polymers, whereas together with light broadening in the peaks, a red shift in their onsets is observed in the range of 26–63 nm. This implies that the aggregation or orderly π–π stacking occurs in the solid state, which is helpful for improving the charge-transport in the film.[7] In addition, in comparison with the absorption spectra in solution, a closer viewing of the spectra revealed that 0–0 vibrational transition decreased, whereas 0–1 increased in both DPP-TVT-1 and DPP-TVT-2 films. It was considered very interesting that the ICT transitions of the polymers were not only blue-shifted, but enhanced intensity of the ICT peaks relative to the corresponding π–π^* transition ones was observed as a function of the increased numbers of thiophene rings. It is evident that the strength of ICT complexes between DPP and TVT units is quite sensitive to the concentration of thiophene spacers. Consequently, the optical bandgaps from the onset absorption of the polymer films follows the order: DPP-TVT-2 > DPP-TVT-1 > DPP-TVT-0, which is an opposite trend in comparison with the magnitude of the π-extension of the donor conjugation, which increases alongside the number of thiophene rings in the repeating unit. Similar phenomena were observed for other bis-lactam-based polymers.[8] Further experiments are currently underway to gain an understanding of the unexpected chromatic shift.

Cyclic voltammetry (CV) was used to investigate the molecular energy levels (HOMO and LUMO) of the three polymers, exhibiting two reversible reductions and a strong quasi-reversible oxidation for all the polymers (see Figure 1c and Table 1). It might be expected that by changing the number of electron-donating thiophene spacers, the HOMOs would be selectively affected, with the LUMOs being almost unchanged.[9] However, the change in the thiophene content in DPP-TVT-n was found to have as significant an influence on the LUMO levels of the polymers as on the HOMO levels; in fact, its effects on the LUMO levels were more pronounced (ranging from −3.55 to −3.23 eV). The LUMOs increased significantly with the number of thiophene spacers, resulting in an increase in the electrochemical bandgaps. This trend coincides closely with the optical bandgaps described above. Ultraviolet photoelectron spectroscopy (UPS) was also used to measure the ionization potential (IP) levels of all the polymers (see Figure 1d). Similar variation trends were found, further confirming the CV results.

Through B3LYP/6–31G calculation on the trimer length oligomers, the theoretical molecular orbital distributions of the optimized structures for the polymer series were visualized; this is illustrated collectively in Figure 1e. In addition to the high coplanarity for all cases, the electron densities of the HOMO and LUMO for DPP-TVT-0-based model are both well delocalized over the conjugated repeat unit, whereas the trimeric systems for DPP-TVT-1 and DPP-TVT-2 demonstrated a similar density of states distribution for both the HOMO and LUMO wave functions. The HOMO levels were well spread across the whole of the molecules with the LUMOs being mostly localized on the DPP acceptors.

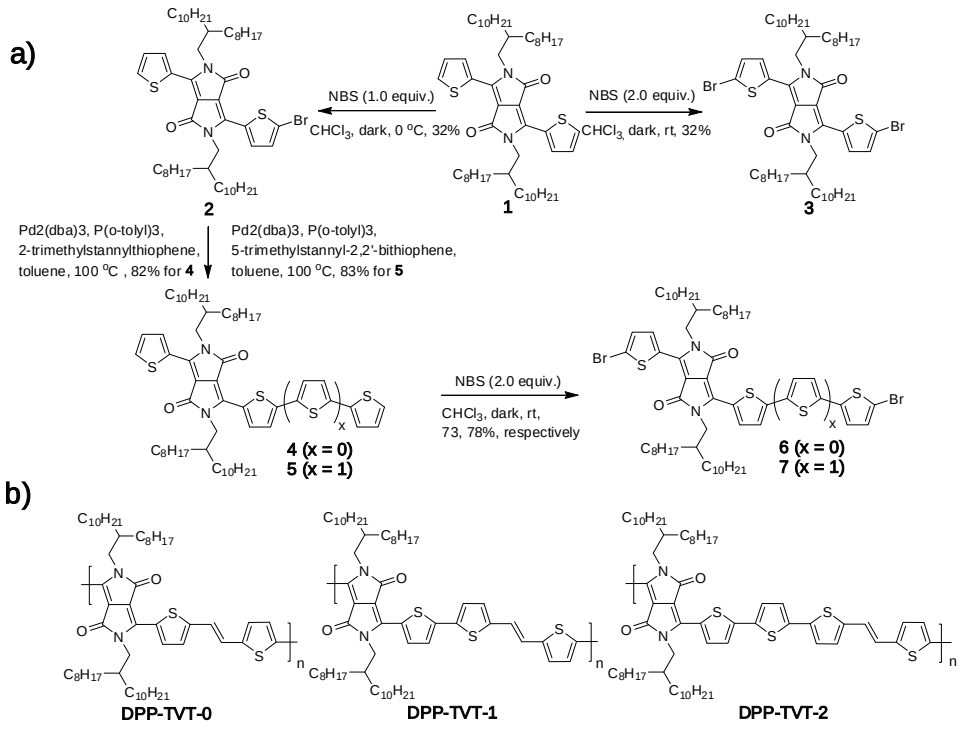

Polymer	Condition	Monomer (Yield %)
DPP-TVT-0	*trans*-1,2-bis(tributylstannyl)ethylene, $Pd_2(dba)_3$, P(*o*-tolyl)$_3$, toluene, 120 °C	3 (67%)
DPP-TVT-1		6 (61%)
DPP-TVT-2		7 (56%)

Scheme 1. a) Synthetic routes of monomers and b) chemical structures of DPP-TVT-n.

2.3. Electrical Characterization and Performance of OFETs

Top-gate/bottom-contact (TG/BC) OFETs were fabricated using DPP-TVT-n polymers as the active layer. The TG/BC OFETs were fabricated on glass substrates without any surface treatment. The semiconducting layers were deposited on the pre-patterned Ni/Au ($t \approx 3$ nm/$t \approx 13$ nm) source and drain electrodes by spin coating of the polymer solutions (5 mg mL^{-1}) in 1,2,4-trichlorobenzene (TCB) at 1000 rpm for 30 s in a nitrogen-filled glove box (oxygen and moisture <10 ppm). The devices were then annealed at temperatures ranging between 150 and 250 °C on a hot plate for 30 min in the same glove box. Subsequently, ≈500 nm-thick PMMA (C_i = 6.20 nF cm^{-2}) was deposited to create a gate-dielectric layer, and the devices were then baked at 80 °C for 1 h. All devices had a channel width (W) of 1000 µm and a channel length (L) of 10–50 µm, respectively. Details of the fabrication of the devices are included in the Experimental section. The output and transfer curves data for all devices are illustrated in Figure 3, and S1–3, and the extracted electrical parameters of the OFETs are listed in **Table 2**, and S1. Upon annealing at a temperature of 200 °C, the electrical performance of all the devices was improved significantly, demonstrating the highest value in average hole mobilities ($\mu_{h,avg}$) from DPP-TVT-n OFETs, as indicated in **Figure 2**. In particular, DPP-TVT-0 was significantly affected by the temperature during the annealing process. However, in the cases of

Table 1. Molecular weights, and optical and electrochemical properties of the DPP-TVT-n polymers.

Polymer	M_n [kDa]/PDI	E_{HOMO} [eV][b]	E_{LUMO} [eV][b]	E_{IP}^{UPS} [eV][c]	$\lambda_{max}^{solution}$ [nm]	$\lambda_{max}^{thinfilm}$ [nm]	E_g^{opt} [eV][a]
DPP-TVT-0	48.4/2.0	−5.28	−3.55	4.94	811, 887	819, 903	1.22
DPP-TVT-1	49.2/1.9	−5.18	−3.39	4.83	760, 808	758, 812	1.34
DPP-TVT-2	23.5/2.9	−5.13	−3.23	4.80	723	720	1.37

[a]Calculated from the absorption band edge of the polymer film, $E_g^{opt} = 1240/\lambda_{edge}$; [b]Thin films in *n*-$Bu_4NPF_6/CH_3CN$, versus ferrocene/ferrocenium at 100 mVs^{-1}. HOMO and LUMO estimated from the onset oxidation and reduction potentials, respectively, assuming the absolute energy level of ferrocene/ferrocenium to be 4.8 eV below vacuum; [c] $E_{IP}^{UPS} = h\nu - (E_{cutoff} - E_{HOMO})$, incident photon energy ($h\nu$ = 21.2 eV) for He I.

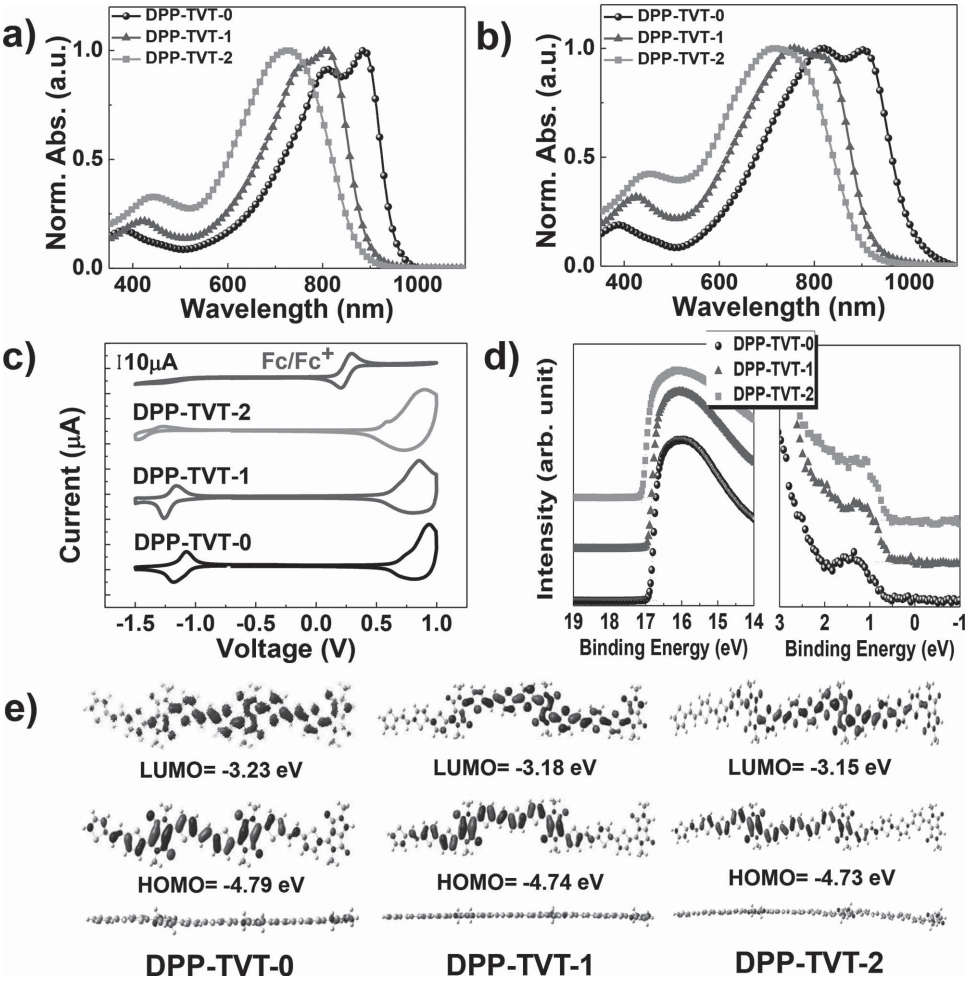

Figure 1. UV–Vis–NIR absorption spectra of DPP-TVT-n (n = 0, 1, 2). a) In dilute chloroform solution and b) as thin films on a quartz plate. c) Cyclic voltammograms of the polymer films in *n*-Bu_4NPF_6/CH_3CN solution (scan rate, 100 mVs^{-1}). d) Ultraviolet photoelectron spectroscopy spectra of all polymers. e) Calculated molecular orbitals and optimized geometries of the trimer oligomers.

DPP-TVT-1 and DPP-TVT-2, the temperature dependence was not as intense as with DPP-TVT-0.

Aside from the flexibility in fabrication and better encapsulation effects resulting from the TG/BC configuration, the top-gate structure is advantageous in achieving a relatively low contact-resistance (R_c) in comparison with other bottom-gated OFET geometry.[10] Consequently, this device configuration was used, and the R_c effect of DPP-TVT-n OFETs was explored by using the Y-function method (YFM) owing to its unique features. This method offers a fast and accurate way to evaluate the contact resistance, because only one transfer sweeping for an individual transistor is required in contrary to commonly used transfer-line method (TLM) with various channel lengths. Therefore, the YFM is suitable for extracting the contact resistance of individual transistors. Although R_c in YFM method is supposed to be closely constant with the gate voltage (V_{GS}), of which assumption is not actually matched to TLM, the values from YFM method almost exist in the error ranges of TLM results proving its accuracy.[11]

Consequently, with the aid of YFM, the R_c is extracted from the transfer characteristics at very low drain voltage (V_{DS} = –10 or 10 V) using Equations 1–5:

$$g_m = \left.\frac{\partial I_{DS}}{\partial V_{GS}}\right|_{V_{DS}=\text{const}} \quad (1)$$

$$Y = \frac{I_{DS}}{\sqrt{g_m}} = \sqrt{\frac{W}{L} C_i \mu_0 V_{DS}} \times (V_{GS} - V_T) \quad (2)$$

$$Sy = \frac{1}{\sqrt{g_m}} \quad (3)$$

$$\theta = \frac{m(Sy)}{m(Y)} \quad (4)$$

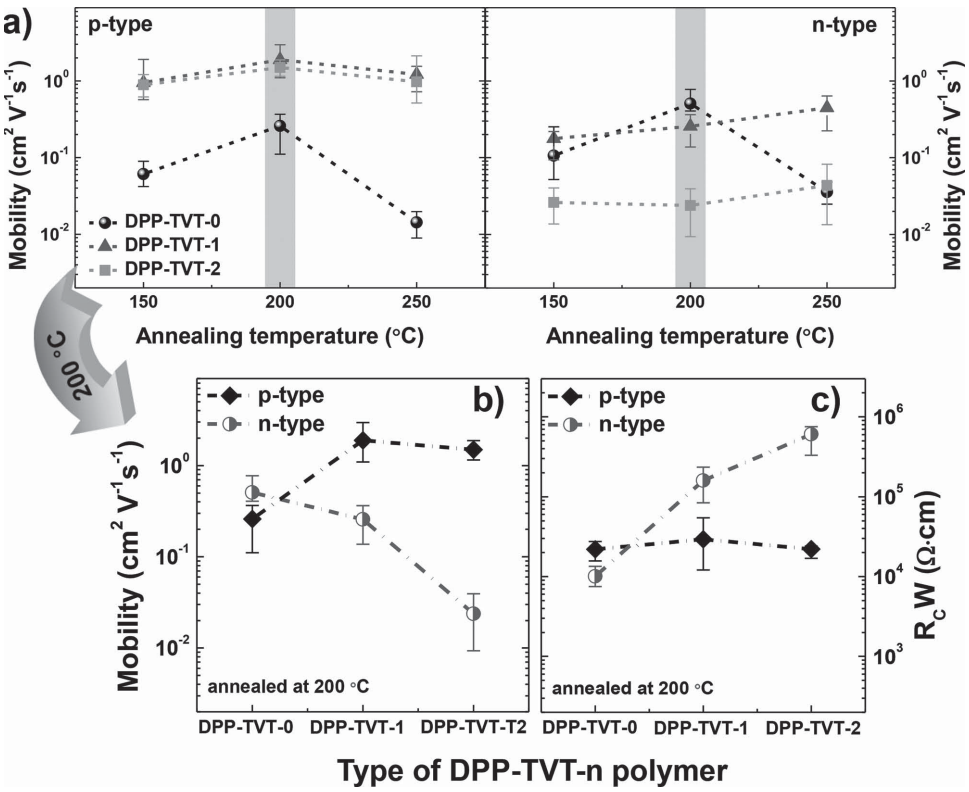

Figure 2. a) Hole and electron charge carrier mobilities for DPP-TVT-n (n = 0, 1, 2) semiconductors based on the annealing temperatures (150, 200, and 250 °C) (left panel: *p*-type and right panel: *n*-type characteristic). The summarized hole and electron b) charge mobilities, and c) channel-width normalized contact resistances (R_cW) for DPP-TVT-n OFETs at an annealing temperature of 200 °C, with the number of flanked thiophene units (n; n = 0, 1, 2).

$$R_c = \frac{\theta}{[m(Y)]^2 / V_{DS}} \quad (5)$$

where C_i is the capacitance of the gate dielectric per unit area, g_m is the transconductance, μ_0 is the low-field mobility, θ is the mobility attenuation factor, $m(Sy)$ and $m(Y)$ are the slopes of Sy and Y (ordinates) against V_{GS} (abscissa) respectively at strong accumulation in linear regime. I_{DS} and V_T are the drain current and the threshold voltage, respectively. Therefore, one can extract the contact resistance by plotting the transconductance (g_m) versus the gate voltage (V_{GS}) where the decreasing tendency, namely the mobility attenuation factor (θ), incorporates the influence of the contact resistance on the effective mobility.

As a result from YFM, the channel-width normalized contact resistance (R_cW) for electrons was found to be increased with the addition of the thiophene units. The DPP-TVT-2 devices clearly demonstrated the largest electron contact resistances of 6.07×10^5 Ω cm on average, as indicated in Figure 2c. This steady increase in the electron contact resistances with the number of flanked thiophene units can be ascribed to the gradually high-lying LUMO energies (see Table 1). Consequently, the relatively deep-lying LUMO energy (−3.55 eV) of DPP-TVT-0 among three polymers, facilitated the most efficient electron injection from the Au electrode owing to its low injection barrier, resulting in the lowest electron contact resistance amongst the OFETs. Correspondingly, together with a structurally synergistic effect of combining fused DPP units and vinylene linkages for their levels of co-planarity, the suitable positions of the LUMO energy levels of these DPP-TVT-n polymers contributed to the effective electron charge injection and transport. Therefore, the decreased number of electron-donating thiophene spacer units (from 2 to 0) led to a noticeable

Table 2. Summary of the electrical OFET characteristics for DPP-TVT-T0, DPP-TVT-1 and DPP-TVT-2 in top-gate/bottom contact configurations at the optimum annealing temperature (T_a = 200 °C).

Condition	*p*-channel			*n*-channel		
Polymers	$\mu_{h,max}$ [cm² V⁻¹s⁻¹]	$\mu_{h,avg}$ [a)] [cm² V⁻¹ s⁻¹]	V_{th} [V]	$\mu_{e,max}$ [cm² V⁻¹ s⁻¹]	$\mu_{e,avg}$ [a)] [cm² V⁻¹ s⁻¹]	V_{th} [V]
DPP-TVT-0	0.37	0.26 (±0.07)	−52 to −65	0.78	0.51 (±0.11)	55–60
DPP-TVT-1	2.96	1.89 (±0.60)	−52 to −77	0.36	0.26 (±0.07)	55–70
DPP-TVT-2	1.88	1.50 (±0.36)	−48 to −69	0.04	0.024 (±0.014)	61–68

[a)]Standard deviations for charge mobilities are indicated in parentheses. All electrical characteristics were obtained from the top-gate based transistors more than ten.

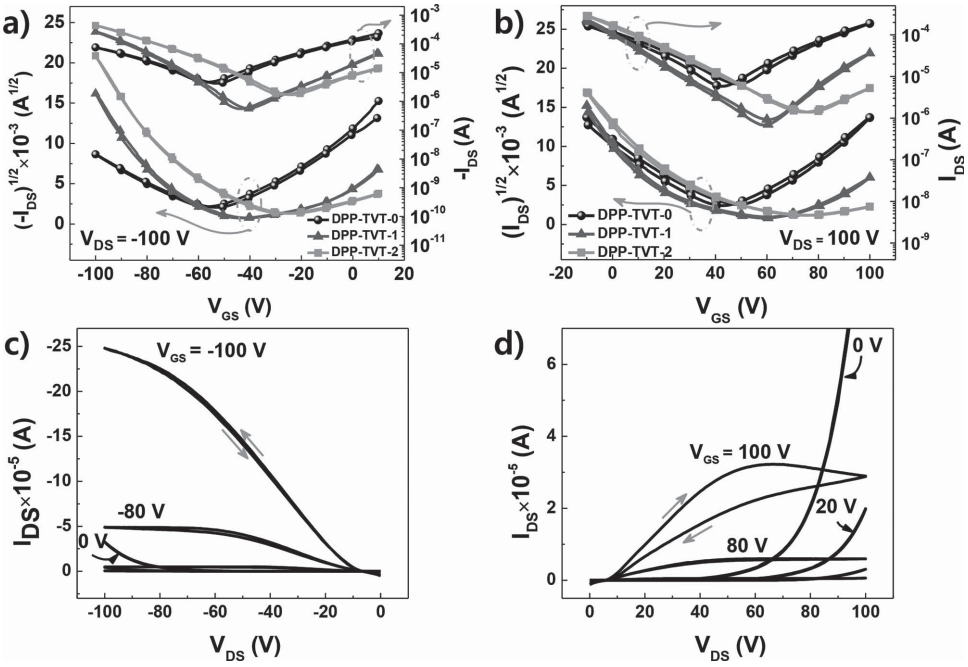

Figure 3. a) Transfer characteristics in the *p*-channel, and b) *n*-channel operation modes of DPP-TVT-n series ambipolar transistor devices (T_a = 200 °C). The corresponding output characteristics of DPP-TVT-1 OFETs annealed at 200 °C for c) *p*- and d) *n*-type modes. (Channel length and width were 20 μm and 1000 μm, respectively.)

improvement in the electron mobilities. Consequentially, DPP-TVT-0 exhibits high average balanced hole and electron mobilities of 0.26 cm^2 V^{-1} s^{-1} and 0.51 cm^2 V^{-1} s^{-1}, respectively. The maximum mobilities for DPP-TVT-0 reached 0.37 cm^2 V^{-1} s^{-1} for holes and 0.77 cm^2 V^{-1} s^{-1} for electrons.

However, the differences between the HOMO energies were not very large in DPP-TVT-n semiconductors, exhibiting a maximum difference of 0.15 eV between DPP-TVT-0, and DPP-TVT-2. Alongside this tendency, the contact resistances for hole injection in DPP-TVT-n were nearly consistently in the range 1.21×10^4–5.43×10^4 Ω cm; this was despite the DPP-TVT-1 and DPP-TVT-2 devices recording better average hole mobilities of 1.89 and 1.50 cm^2 V^{-1} s^{-1}, respectively, in comparison with DPP-TVT-0 ($\mu_{h,avg}$ = 0.26 cm^2 V^{-1} s^{-1}). The maximum hole mobility, 2.96 cm^2 V^{-1} s^{-1}, was observed with DPP-TVT-1.

Figure 3 plots the representative transfer and output characteristics of optimized DPP-TVT-based polymer OFETs and their performances. Despite the similar HOMO levels and contact resistances among the three polymers, the remarkably soaring hole mobilities for DPP-TVT-1 and DPP-TVT-2 could have arisen from the different solid-state ordering, degree of planarity, and molecular packing properties in the polymer backbones at the semiconductor–insulator interfaces. Therefore, the following section includes a discussion and comparison of the semiconductor packing structures and their crystallite distributions in terms of their electrical performances through comprehensive X-ray analysis.

2.4. Microstructure Analyses

In order to gain a greater understanding of the correlation between the crystalline microstructures and the charge transport properties, grazing-incidence X-ray diffraction (GIXD) experiments of both as-spun and annealed DPP-TVT-n thin films were performed. The annealing temperatures of DPP-TVT-0, DPP-TVT-1, and DPP-TVT-2 were all fixed at 200 °C, at which each sample demonstrated the best electrical properties. For as-spun thin film samples DPP-TVT-0, DPP-TVT-1, and DPP-TVT-2, first diffraction peaks (*100*) were observed in X-ray scattering patterns (out-of-plane) at q_z = 0.2898 Å^{-1}, 0.2824 Å^{-1}, and 0.3164 Å^{-1}, with interlayer distances (d_{100}) of 21.68 Å, 22.25 Å, and 19.86 Å, respectively (Figure S4~S5). In the all non-annealed samples, the interlayer and the (*010*) diffraction attributing to π–π stacking peaks were observed at both the out-of-plane and in-plane profiles, thus confirming a mixture of face-on and edge-on orientations. An annealing-induced improved crystallinity was observed for all polymers after annealing at 200 °C; the films displayed higher intensity (*100*) diffraction peaks and multi-peaks diffraction (see **Figure 4**). Such an increase in long-range ordering could be an important factor in the origins of their high mobilities upon annealing. More interestingly, the (*010*) diffraction peaks were weakened or disappeared at the out-of-plane GIXD profiles after annealing (see Figure S4 for 1D-GIXD), especially in the annealed DPP-TVT-1 and DPP-TVT-2 films, implying the favored orientation change from the face-on structure to the edge-on structure. In addition, atomic force microscopy (AFM) images indicated that, after annealing at 200 °C, all polymer films were filled with the uniformity that affords homogeneous structures. Notably, the intertwined polymer fibers were observed for the annealed DPP-TVT-2 film surfaces (see Figure S6).

Furthermore, in the case of the annealed samples, as the number of thiophene spacers in the backbone increased, both (*h00*) diffractions representing lamellar packing and (*010*)

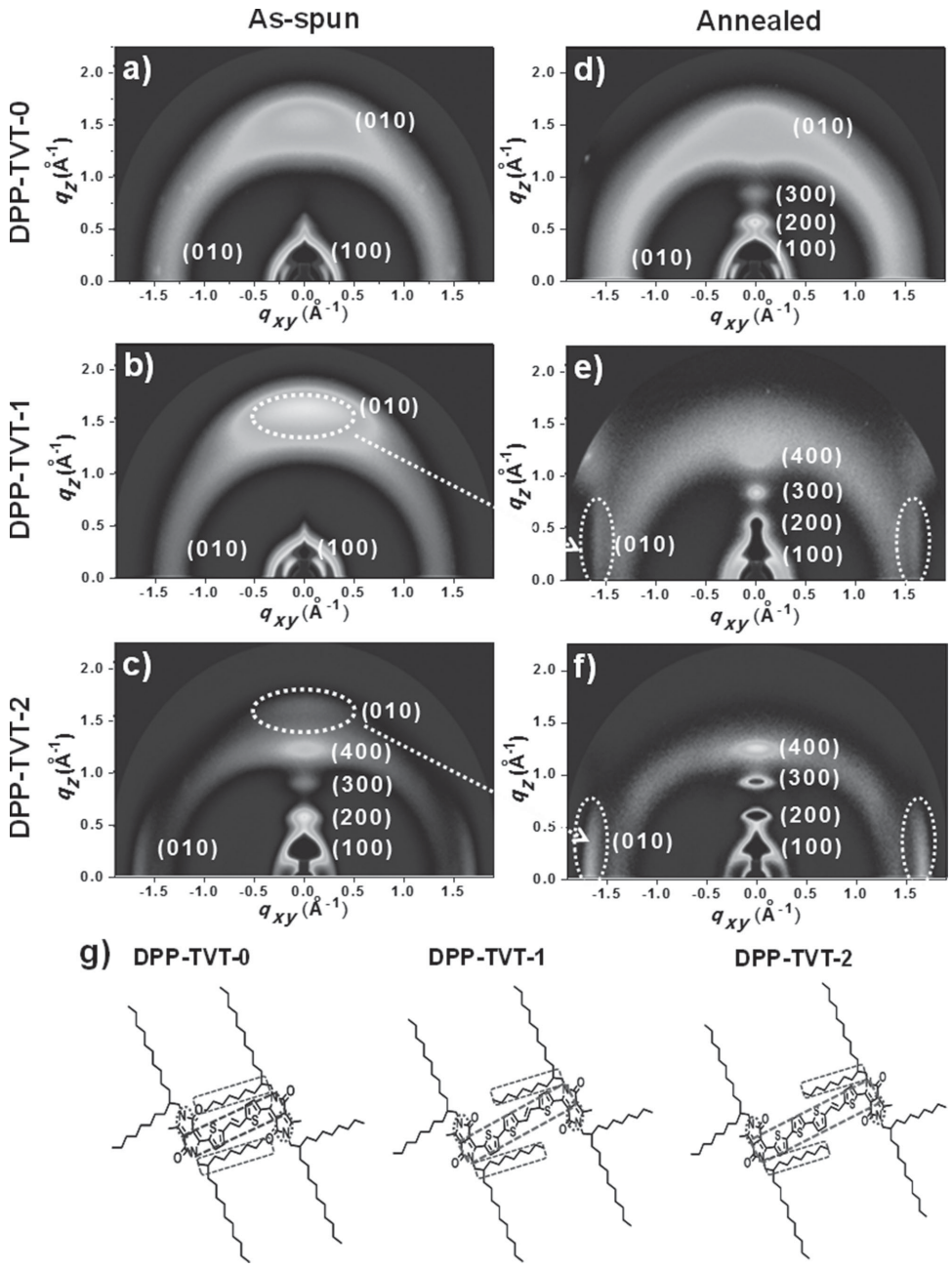

Figure 4. Grazing incidence X-ray diffraction (GIXD) images of a–c) as-spun and d–f) annealed DPP-TVT-n (n = 0, 1, 2) thin films. The annealing temperature of (d–f) were 200 °C. g) Proposed molecular packing of the DPP-TVT-n.

diffraction became more distinctively observed. Owing to the charge transport/transfer being believed to be facilitated by strong π–π stacking, the structures of DPP-TVT-1 and DPP-TVT-2 having clear (*010*) diffraction can be considered as favorable molecular conformation of high hole/electron transport, in comparison with that of DPP-TVT-0. As schematically illustrated in Figure 4g, it is postulated that the enhanced lamellar packing and π–π stacking for both DPP-TVT-1 and DPP-TVT-2 result from the large distances between DPP motifs in a single repeat unit, thereby allowing the branched side chains (2-octyldodecyl group) to pack properly along the backbone without steric hindrance. Conversely, the reduced distance arising from the absence of the thiophene spacers in DPP-TVT-0 might perturb the alignment of the side chains to the direction of the backbone, resulting in less ordered molecular organization. Details of the layer spacing (d_{100}) and π–π stacking distance (d_{010}) for the annealed films are summarized in **Table 3**. Obviously, the shortest lamellar spacing and the smallest π–π stacking distance for DPP-TVT-2 are observed, indicating the more densely packed/ordered microstructure. These intriguing results challenge the traditional assumption that high carrier mobility is unambiguously linked to the

Table 3. Crystallographic parameters of the annealed DPP-TVT-n (n = 0, 1, 2) thin films at the optimum annealing temperature (T_a = 200 °C).

Polymer	[a] $d_{(100)}$ [Å]	[b] $d_{(010)}$ [Å]	[c] $\overline{L}_{(h00)}$ [Å]	[d] $\overline{N}_{(h00)}$	[e] $g_{(h00)}$ [%]
DPP-TVT-0	20.87	3.89	103.0	4.9	4.9
DPP-TVT-1	20.91	3.84	144.9	7.0	3.8
DPP-TVT-2	19.53	3.80	202.0	10.7	4.0

[a] Layer spacing (or domain spacing) of the plane; [b] π–π stacking distance extracted from in-plane direction; [c] True paracrystal size normal to the (*h00*) plane; [d] The average number of the (*h00*) plane; [e] The paracrystalline distortion parameter of the (*h00*) plane.

degree of order, a paradigm that has been successfully used in the past to describe charge transport in older semiconducting polymers.[12]

In aiming to uncover the inconsistency between OFET device performance and π–π stacking distances in the polymers, distortion parameter and plane distribution were examined. Paracrystals are known to be the building blocks of many condensed matters, including polymers and biological materials; consequently, assessment of the paracrystalline nature of the DPP-TVT-n thin films should prove quite useful in correlating with charge transport properties. The paracrystalline distortion parameter (g), defined as the statistical standard deviation from its average lattice position, can be calculated from the slope (= $g^2\pi^2/d$; d is the domain spacing) of the δb–h^2 plot, where δb is the integral widths of the diffraction peaks calculated from $\delta b = 1/L_c$ (L_c: coherence length or paracrystal size) and h is the order of diffractions.[13] Furthermore, the true paracrystal size ($\overline{L}_C$) can be obtained from the intercept of the straight line with the ordinate. Additionally, the average number of the diffraction plane ($\overline{N}$) can be calculated from ($\overline{L}_C$) = $\overline{N}$ d. The δb–h^2 curves of the annealed DPP-TVT-n thin films extracted from GIXD data are included in **Figure 5**a and the crystallographic parameters are listed in Table 3. The calculated paracrystalline distortion parameter (g) values of DPP-TVT-0, DPP-TVT-1 and DPP-TVT-2 were found to be 4.9, 3.8, and 4.0%, respectively. Additionally, the average numbers of the diffraction plane ($\overline{N}$) of DPP-TVT-0, DPP-TVT-1 and DPP-TVT-2 were 4.9, 7.0, and 10.7 layers, respectively.

An intensity-corrected pole figure plot along the (*200*) diffraction peak of the annealed DPP-TVT-n thin films is displayed in Figure 5b; these data imply the degree of distribution of (*h00*) plane. DPP-TVT-1 exhibited the narrowest (*h00*) plane distribution (FWHM = 6.8°), while DPP-TVT-0 (FWHM = 12.4°) and DPP-TVT-2 (FWHM = 11.1°) exhibited a distribution approximately two-times wider. When considering that DPP-TVT-1 has a relatively smaller paracrystalline nature and narrower (*h00*) plane distribution, consisting of a moderate number of diffraction plane ($\overline{N} \approx 7$), in comparison with those of DPP-TVT-0 and DPP-TVT-2, this type of molecular organization is regarded particularly favorable for charge carrier. This is proposed to be the primary reason for the observed highest hole mobility of DPP-TVT-1, despite the aforementioned larger π–π stacking distance relative to DPP-TVT-2.

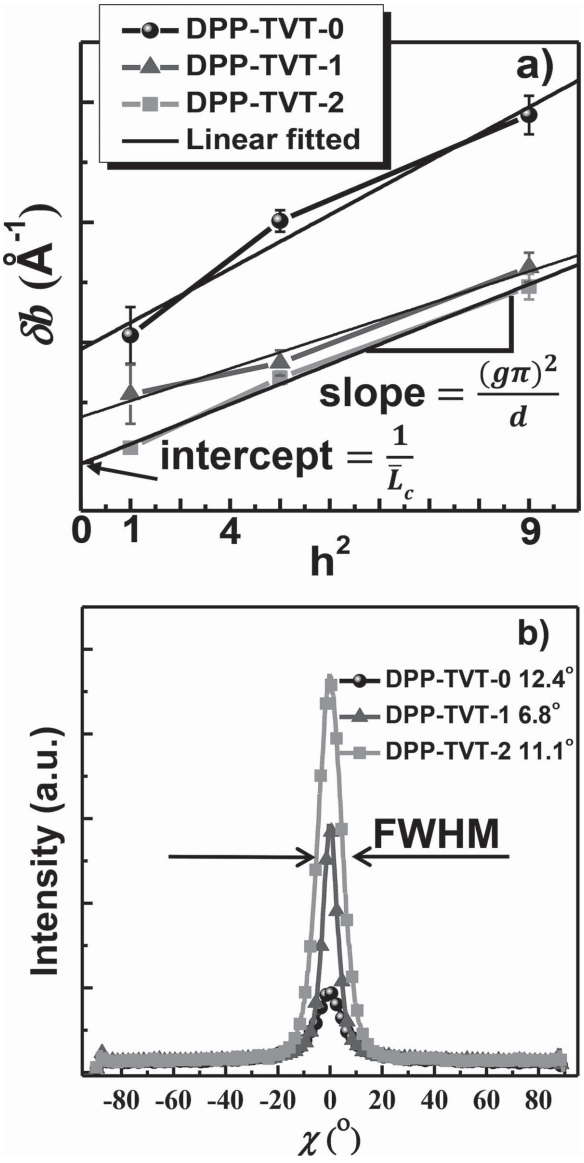

Figure 5. a) δb–h^2 curves of the annealed DPP-TVT-n (n = 0, 1, 2) thin films extracted from GIXD analysis. The error bar is the standard deviation from a different set of measurements. b) Intensity corrected pole figure plot along the (*200*) diffraction peak of the annealed DPP-TVT-n (n = 0, 1, 2) thin films, where (*200*) the diffraction peak was chosen for the pole figure plot in order to minimize the surface scattering effects resulting from the substrate.

3. Conclusion

With recent advances in the mobility of TVT-like polymers, a systematic study of a tactical synthesized series of D–A polymeric hybrids (DPP-TVT-n) containing DPP and TVT, and the different number of thiophene spacers was conducted with the aim of establishing parallels and trends between TVT-based structures and OFET performance. As demonstrated by optical and electrochemical analyses, upon lowering the thiophene content between DPP and TVT building blocks, the absorption spectra not only exhibited obvious red-shift, but a stepwise increase in both LUMO and HOMO levels was also observed;

however, the LUMOs were clearly more easily affected. When considering the size of the electron-donating moieties in the polymer repeating unit, the variations in the energy levels of the polymers do not follow a common tendency previously observed in the literature. The utilization of the DPP-TVT-n in OFETs leads to the achievement of ambipolar charge transport. DPP-TVT-0 exhibited nearly balanced hole and electron mobilities of 0.37 and 0.78 $cm^2\ V^{-1}\ s^{-1}$, respectively. Of particular significance is that OFETs based on the polymers, regardless of the variation in LUMO levels, appeared to tune the polarity of charge carriers with an increase in hole mobilities as they adopt thiophene spacers, resulting in *p*-type dominant ambipolar transport characteristics for DPP-TVT-1~2. Among the polymers, even though DPP-TVT-2 has the shortest value in both lamellar *d*-spacing and π-stacking distance, DPP-TVT-1 demonstrated the highest hole mobility (up to 2.96 $cm^2\ V^{-1}\ s^{-1}$). Based on the results in this study, it can be concluded that the degrees of the paracrystalline nature and the (*h00*) plane distribution also play a critical role in improving hole mobilities. These findings should help not only to move towards the rationalization of structure–property relationships in a relevant class of TVT-like polymer semiconductors, but also to provide a new test bench for charge-transport mechanisms, assisting in the design of top-performing semiconducting polymers.

4. Experimental Section

All chemicals materials were purchased from Aldrich and Alfa and were used without further purification. All solvents were ACS and anhydrous grade by distillation. 2-trimethylstannylthiophene, and 5-trimethylstannyl-2,2′-bithiophene were synthesized according to a method reported previously in the literature.[14] ^{1}H NMR and ^{13}C NMR spectra were recorded using an Agilent 400 MHz spectrophotometer with $CDCl_3$ being used as a solvent and tetramethylsilane (TMS) used as the internal standard; MALDI MS spectra were checked using an Ultraflex III (Bruker, Germany) system. UV–Vis–NIR spectra were recorded using a UV-1800 (SHIMADZU) spectrophotometer. DFT calculations were performed using the Gaussian 09 package with the nonlocal hybrid Becke three-parameter Lee-Yang-Parr (B3LYP) function and the 6–31G basis was set to elucidate the HOMO and LUMO levels after optimizing the geometry of DPP-TVT-0, DPP-TVT-1, and DPP-TVT-2 using the same method. The number-average (M_n) and weight average (M_w) molecular weights, and the polydispersity index (PDI) of the polymer products were determined by performing gel permeation chromatography (GPC) with a Perkin-Elmer Series 200 system using a series of mono disperse polystyrene standards in THF (HPLC grade) at 313 K. Cyclic voltammetry (CV) measurements were performed on (METEK, Versa STAT3) with a three-electrode cell in 0.1 M tetra-*n*-butylammonium hexafluorophosphate (n-Bu_4NPF_6) solution in acetonitrile, using a scan rate of 100 mV/s at room temperature under nitrogen. Ag/Ag^+, platinum, and glass carbon were used as the reference electrode, counter electrode, and working electrode, respectively. The Ag/Ag^+ reference electrode was calibrated using a ferrocene/ferrocenium redox couple as an internal standard, with the oxidation potential set at −4.8 eV with respect to a zero vacuum level. The HOMO energy levels were obtained from the equation HOMO (eV) = $-$ ($E_{(ox)}^{onset} - E_{(ferrocene)}^{onset} + 4.8$) and the LUMO levels were calculated from the equation LUMO (eV) = $-$ ($E_{(red)}^{onset} - E_{(ferrocene)}^{onset} + 4.8$). Ultraviolet photoelectron spectroscopy (UPS) was examined using an AXIS-NOVA CJ109 system (Kratos). The polymer solution was prepared in 5 mg mL^{-1} chlorobenzene for DPP-TVT-0, DPP-TVT-1, and DPP-TVT-2. A gold film with a thickness of 75 nm was deposited on a pre-cleaned Si substrate with a thin native oxide. The DPP-TVT-0, DPP-TVT-1, and DPP-TVT-2 solutions were spin-coated onto gold films. Film fabrication was performed in a N_2-atmosphere glovebox. The UPS analysis chamber was equipped with a hemispherical electron-energy analyzer (Kratos Ultra Spectrometer), and the chamber was maintained at 3.00×10^{-9} Torr. The UPS measurements were performed using the He I ($h\nu$ = 21.2 eV) source.

Morphology Analyses: Atomic force microscopy (AFM) images were collected using a Digital Instruments dimension AFM system, controlled by a nanoscope scanning probe microscope controller. Two-dimensional Grazing incidence X-ray diffraction (2D-GIXD) measurements were performed at the PLS-II 9A U-SAXS beamline of the Pohang Accelerator Laboratory in Korea. The X-rays emitted from the in-vacuum undulator (IVU) were monochromated (E_k = 11.09 keV, λ = 1.118 Å) using a Si(*111*) double-crystal monochromator and were focused horizontally and vertically (300 (*H*) μm × 30 (*V*) μm in FWHM at the sample position) using a K-B type focusing mirror system. The GIXD sample stage was equipped with a 7-axis motorized stage for the fine alignment of the thin sample. The incidence angle of X-rays was adjusted to 0.10°, which is just below the critical angle of DPP-TVT-n (n = 0, 1, 2). GIXD patterns were recorded with a 2D CCD detector (Rayonix SX165, USA) and the X-ray irradiation time was 10–20 s. The diffraction angle was calibrated using pre-calibrated sucrose (Monoclinic, P21, a = 10.8631 Å, b = 8.7044 Å, c = 7.7624 Å, β = 102.938°) and the sample-to-detector distance was approximately 226 mm.[15]

Device Fabrication and Characterization: Top-gate/bottom-contact geometry (TG/BC) was applied in the fabrication of the OFET devices. Prior to the fabrication, the glass substrates (Corning Eagle XG) were sequentially cleaned using acetone, isopropanol, and deionized water for 10 min each using a sonication bath. The cleaned substrates were dried in a vacuum oven at a temperature of 110 °C for 20 min. Following this, the source and drain electrodes (Ni/Au = 3/13 nm) were patterned through conventional photolithography processes and Ni and Au were deposited on the glass substrates using thermal-evaporation deposition. The resultant channel lengths were 10, 20, 30 and 50 μm and the width was 1000 μm. The synthesized donor–acceptor DPP-TVT-n polymers were used without further purification. The various semiconductor solutions (DPP-TVT-0, DPP-TVT-1, and DPP-TVT-2) from 5 mg mL^{-1} in 1,2,4-trichlorobenzene (from Sigma Aldrich) were spin-coated at 1000 rpm for 30 s before being thermally annealed at different temperatures within the range 150–250 °C for 30 min in a N_2-purged glove box. After thermal annealing of the semiconductors, poly(methyl methacrylate) (PMMA; average M_w: 120kDa, purchased from Sigma Aldrich) film was spin-coated from 80 mg mL^{-1} solution in *n*-butyl acetate before being baked at 80 °C for 1 h in an N_2-purged glove box as gate dielectric layers with a thickness of ≈500 nm (capacitance: 6.20 nF cm^{-2}). Finally, the transistors were completed by depositing top-gate aluminum electrodes (≈50 nm) via thermal evaporation with a metal shadow mask. Every OFET device was characterized using a Keithley 4200-SCS semiconductor parameter analyzer connected to a probe station in an inert N_2-glove box.

Synthesis of 2,5-bis(2-octyldodecyl)-3,6-di(thiophene-2-yl)pyrrolo[3,4-c]pyrrole-1,4-dione (1): A solution of 2-octyldodecyliodide (16.9 g, 41.6 mmol) was added dropwise to a mixture of 3,6-bis(thiophen-2-yl)-2*H*,5*H*-pyrrolo[3,4-*c*]pyrrole-1,4-dione (5.0 g, 16.6 mmol), K_2CO_3 (5.75 g, 41.6 mmol) in anhydrous DMF (100 mL). The mixture was maintained at 120 °C overnight. The reaction was cooled to room temperature and evaporated under reduced pressure. The compound was extracted in CH_2Cl_2, washed with brine, and dried over $MgSO_4$. The crude product was purified by chromatography on silica with 0–50% dichloromethane in hexane used as an eluent. The isolated yield was 7.02 g (49%) as a bright pink-red solid.

Synthesis of 3-(5-bromothiophene-2-yl)-2,5-bis(2-octyldodecyl)-6-(thiophene-2-yl)pyrrolo[3,4-c]pyrrole-1,4-dione (2): *N*-Bromosuccinimide (NBS, 1.03 g, 5.80 mmol) in $CHCl_3$ (100 mL) was added to a solution of 2,5-bis(2-octyldodecyl)-3,6-di(thiophen-2yl)pyrrolo[3,4-*c*]pyrrole-1,4-dione (**1**) (2 g, 2.32 mmol) at 0 °C over the course of 6 h. The reaction was stirred at room temperature overnight and the solvent was removed under reduced pressure. The crude product was purified using chromatography on silica with 0–50% dichloromethane in hexane

utilized as the eluent. The isolated yield was 2.5 g (32%) as a bright purple solid. ^{1}H NMR (400 MHz, $CDCl_3$, δ): 8.88 (d, J = 4 Hz, 1H), 8.61 (d, J = 4 Hz, 1H), 7.63 (d, 1H), 7.27 (d, J = 5.2 Hz, 1H), 7.22 (d, J = 4.4 Hz, 1H), 3.99–3.89 (m, 4H), 1.89–1.87 (m, 2H), 1.27–1.21 (m, 64H), 0.88–0.83 (m, 12H). ^{13}C NMR (100 MHz, $CDCl_3$, δ): 161.57, 161.43, 140.84, 138.89, 135.50, 135.02, 131.31, 131.27, 130.71, 129.76, 128.42, 118.53, 108.13, 107.76, 46.25, 37.74, 37.71, 31.92, 31.87, 31.32, 31.16, 30.05, 29.99, 29.63, 29.56, 29.54, 29.48, 29.35, 29.28, 26.33, 26.18, 22.68, 22.66, 14.10. MALDI-TOF MS(m/z) 937 (M^+). Anal. calcd. for $C_{54}H_{87}BrN_2O_2S_2$: C, 68.97; H, 9.33; Br, 8.50; N, 2.89; O, 3.40; S, 6.82; found: C, 68.69; H, 9.36; N, 2.88; O, 3.57; S, 6.55.

Synthesis of 3,6-bis(5-bromothiene-2-yl)-2,5-bis(2-octyldodecyl)pyrrolo[3,4-c]pyrrole-1,4-dione (3): NBS (0.95 g, 5.34 mmol) was added slowly to a solution of 2,5-bis(2-octyldodecyl)-3,6-di(thiophene-2-yl)pyrrolo[3,4-*c*]pyrrole-1,4-dione (**1**) (1 g, 2.32 mmol) in $CHCl_3$ (100 mL). The solution was protected from light and stirred at room temperature overnight. The reaction mixture was poured into water (100 mL) and extracted in $CHCl_3$. The organic layer was dried over $MgSO_4$ and the solvent was evaporated under reduced pressure. The crude product was purified by chromatography on silica with 0–50% dichloromethane in hexane used as an eluent. The isolated yield was 1.82 g (77%) as a purple solid. The ^{1}H NMR assignment was in full agreement with that previously reported one.[3h]

Synthesis of 2,5-bis(2-octyldodecyl)-3-(thiophen-2-yl)-6-(5-(thiophen-2-yl)thiophen-2-yl)pyrrolo[3,4-c]pyrrole-1,4-dione (4): 3-(5-bromothiophene-2-yl)-2,5-bis(2-octyldodecyl)-6-(thiophene-2-yl)pyrrolo[3,4-*c*]pyrrole-1,4-dione (**2**) (1.1 g, 1.17 mmol), 2-trimethylstannylthiophene (0.29 g, 1.17 mmol), tri(*o*-tolyl)phosphine (P(*o*-tolyl)$_3$, 35.6 mg, 0.117 mmol) in toluene (10 mL) were filled in a microwave reactor vial. After the mixture was purged for 30 min, tris(dibenzylideneacetone)dipalladium(0) ($Pd_2(dba)_3$, 53.5 mg, 0.058 mmol) was added to the solution mixture. The mixture was heated at 100 °C for 1 h in a microwave reactor, and reaction was cooled to room temperature. The solvent was removed under reduced pressure. The crude product was purified by chromatography on silica with 0–50% dichloromethane in hexane used as an eluent. The isolated yield was 0.9 g (82%) as a purplish solid. ^{1}H NMR (400 MHz, $CDCl_3$, δ): 8.92 (dd, J = 3.2, 2.4 Hz, 2H), 7.59 (d, J = 4.8 Hz, 1H), 7.30–7.27 (m, 3H), 7.25–7.22 (m, 1H), 7.06–7.03 (m, 1H), 4.01–3.89 (m, 4H), 1.95–1.91 (m, 2H), 1.29–1.21 (m, 64H), 0.87–0.82 (m, 12H) ppm. ^{13}C NMR (100 MHz, $CDCl_3$, δ): 161.71, 161.55, 142.73, 139.97, 139.86, 136.70, 136.21, 135.13, 130.29, 129.92, 128.35, 128.20, 128.04, 126.18, 125.09, 124.69, 108.12, 108.09, 46.24, 37.92, 37.74, 31.92, 31.89, 31.32, 31.18, 30.05, 30.01, 29.64, 29.61, 29.55, 29.50, 29.36, 29.29, 26.34, 26.20, 22.69, 22.66, 14.11. MALDI-TOF MS(m/z) 941 (M^+). Anal. calcd. for $C_{58}H_{90}N_2O_2S_3$: C, 73.83; H, 9.61; N, 2.97; O, 3.39; S, 10.20; found: C, 73.57; H, 9.39; N, 3.12; O, 3.61; S, 10.56.

Synthesis of 2,5-bis(2-octyldodecyl)-3-(thiophen-2-yl)-6-(5-(5-(thiophen-2-yl)thiophen-2-yl)thiophen-2-yl)pyrrolo[3,4-c]pyrrole-1,4-dione (5): 3-(5-bromothiophene-2-yl)-2,5-bis(2-octyldodecyl)-6-(thiophene-2-yl)pyrrolo[3,4-*c*]pyrrole-1,4-dione (**2**) (0.90 g, 0.957 mmol), 5-trimethylstannyl-2,2'-bithiophene (0.32 g, 0.957 mmol), P(*o*-tolyl)$_3$ (29.1 mg, 0.096 mmol) in toluene (10 mL) were filled in a microwave reactor vial. After the mixture was purged with argon for 30 min, $Pd_2(dba)_3$ (43.8 mg, 0.048 mmol) was added to the solution mixture. The mixture was heated at 100 °C for 1 h in a microwave reactor, and reaction was cooled to room temperature. The solvent was removed under reduced pressure. The crude product was purified by chromatography on silica with 0–50% dichloromethane in hexane used as the eluent. The isolated yield was 1.0 g (83%) as a dark purplish solid. ^{1}H NMR (400 MHz, $CDCl_3$, δ): 8.92 (dd, J = 3.6, 4 Hz, 2H), 7.61 (d, J = 4.4 Hz, 1H), 7.27 (s, 1H), 7.24 (s, 1H), 7.22 (t, J = 6.4 Hz, 2H), 7.12 (d, J = 4 Hz, 1H), 7.05–7.02 (t, J = 9.2 Hz, 1H), 4.03–4.01 (m, 4H), 1.96–1.91 (m, 2H), 1.33–1.21 (m, 64H), 0.89–0.82 (m, 12H) ppm. ^{13}C NMR* (100 MHz, $CDCl_3$, δ): 161.73, 161.54, 142.39, 139.83, 138.23, 136.77, 136.66, 135.13, 134.74, 130.30, 129.93, 128.37, 128.01, 125.77, 125.09, 124.57, 124.54, 124.20, 108.16, 46.26, 37.96, 37.74, 31.92, 31.89, 31.36, 31.18, 30.08, 30.02, 29.69, 29.66, 29.59, 29.50, 29.37, 29.29, 26.39, 26.21, 22.69, 22.67, 14.12. *All possible signals for the sp^2 carbons were difficult to detect separately, because of the overlapping peaks. MALDI-TOF MS(m/z) 1023 (M^+). Anal. calcd. for $C_{62}H_{92}N_2O_2S_4$: C, 72.60; H, 9.04; N, 2.73; O, 3.12; S, 12.51; found: C, 72.70; H, 8.98; N, 2.72; O, 3.01; S, 12.50.

Synthesis of 3-(5-bromothiophen-2-yl)-6-(5-(5-(thiophen-2-yl)thiophen-2-yl)-2,5-bis(2-octyldodecyl)pyrrolo[3,4-c]pyrrole-1,4-dione (6): NBS (0.40 g, 2.23 mmol) was added slowly to a solution of 2,5-bis(2-octyldodecyl)-3-(thiophen-2-yl)-6-(5-(thiophen-2-yl)thiophen-2-yl)pyrrolo[3,4-*c*]pyrrole-1,4-dione (**4**) (1.0 g, 1.05 mmol) in $CHCl_3$ (100 mL). The solution was protected from light and stirred at room temperature overnight. The reaction mixture was poured into water (100 mL) and extracted in $CHCl_3$. The organic layer was dried over $MgSO_4$ and the solvent was evaporated under reduced pressure. The crude product was purified by chromatography on silica with 0–50% dichloromethane in hexane used as the eluent. The isolated yield was 0.85 g (73%) as a wine-color solid. ^{1}H NMR (400 MHz, $CDCl_3$, δ): 8.86 (d, J = 4 Hz, 1H), 8.61 (d, J = 3.6 Hz, 1H), 7.22–7.19 (m, 2H), 7.06 (dd, J = 4, 3.6 Hz, 2H), 3.99–3.91 (m, 4H), 1.90–1.88 (m, 2H), 1.29–1.21 (m, 64H), 0.88–0.83 (m, 12H) ppm. ^{13}C NMR (100 MHz, $CDCl_3$, δ): 161.37, 161.14, 141.56, 139.88, 138.54, 137.61, 136.74, 135.13, 131.28, 131.03, 130.61, 128.29, 125.06, 124.72, 118.62, 113.20, 108.16, 108.08, 46.27, 37.89, 37.74, 31.93, 31.89, 31.32, 31.18, 30.06, 30.00, 29.66, 29.57, 29.52, 29.38, 29.31, 26.34, 26.19, 22.69, 22.68, 22.51, 14.12. MALDI-TOF MS(m/z) 1098 (M^+). Anal. calcd. for $C_{58}H_{88}Br_2N_2O_2S_3$: C, 63.25; H, 8.05; Br, 14.51; N, 2.54; O, 2.91; S, 8.73; found: C, 63.51; H, 8.05; N, 2.58; O, 2.75; S, 9.01.

Synthesis of 3-(5-bromothiophen-2-yl)-6-(5-(5-(5-bromothiophen-2-yl)thiophen-2-yl)-2,5-bis(2-octyldodecyl)pyrrolo[3,4-c]pyrrole-1,4-dione (7): NBS (0.36 g, 2.05 mmol) was added slowly to a solution of 2,5-bis(2-octyldodecyl)-3-(thiophen-2-yl)-6-(5-(5-(thiophen-2-yl)thiophen-2-yl)thiophen-2-yl)pyrrolo[3,4-*c*]pyrrole-1,4-dione (**5**) (1.0 g, 0.975 mmol) in $CHCl_3$ (100 mL). The solution was protected from light and stirred at room temperature overnight. The reaction mixture was poured into water (100 mL) and extracted in $CHCl_3$. The organic layer was dried over $MgSO_4$ and the solvent was evaporated under reduced pressure. The crude product was purified by chromatography on silica with 0–50% dichloromethane in hexane used as an eluent. The isolated yield was 0.9 g (78%) as a navy-color solid. ^{1}H NMR (400 MHz, $CDCl_3$, δ): 8.92 (d, J = 4 Hz, 1H), 8.61 (d, J = 4 Hz, 1H), 7.28 (d, J = 4 Hz, 1H), 7.20 (d, J = 3.6 Hz, 2H), 7.05–6.93 (m, 3H), 3.95–3.90 (m, 4H), 1.88 (m, 2H), 1.330–1.22 (m, 64H), 0.87–0.82 (m, 12H) ppm. ^{13}C NMR* (100 MHz, $CDCl_3$, δ): 161.43, 161.09, 142.29, 139.95, 138.27, 138.07, 137.06, 135.10, 134.09, 131.31, 130.82, 130.64, 128.11, 125.75, 124.68, 124.17, 118.51, 111.87, 108.23, 107.99, 46.27, 37.89, 37.74, 31.93, 31.89, 31.32, 31.18, 30.06, 30.00, 29.66, 29.57, 29.52, 29.38, 29.31, 26.34, 26.19, 22.69, 22.68, 22.51, 14.12. *All possible signals for the sp^2 carbons were difficult to detect separately, because of the overlapping peaks. MALDI-TOF MS(m/z) 1180 (M^+). Anal. calcd. for $C_{62}H_{90}Br_2N_2O_2S_4$: C, 62.92; H, 7.67; Br, 13.50; N, 2.37; O, 2.70; S, 10.84; found: C, 62.87; H, 7.59; N, 2.17; O, 2.85; S, 10.76.

Typical Procedure for Stille Polymerization and Polymer Purification: Dibrominated DPP (**3**, **6**, or **7**) (0.196 mmol), *trans*-1,2-bis(tributylstannyl) ethylene (0.196 mmol), P(*o*-tolyl)$_3$ (19.6 µmol), and anhydrous toluene (5 mL) were mixed in a Schlenk flask that had been purged with argon for 30 min. To this solution, $Pd_2(dba)_3$ (9.81 µmol) was added and the reaction was subsequently heated to 120 °C and stirred for 48 h. The crude product was precipitated in methanol (200 mL). The precipitate was collected into a Soxhlet thimble and sequential Soxhlet extraction with methanol (1 day), acetone (1 day), hexane (1 day), and finally chloroform (1 day) was performed. The final chloroform solution was concentrated and precipitated in methanol. The final product was filtered and drying in *vacuo*.

Synthesis of Poly(2,5-bis(2-octyldodecyl)-3,6-di(thiophen-2-yl)pyrrolo[3,4-c]pyrrole-1,4-dione)-alt-1,2-vinyl-5,5'-diyl) (DPP-TVT-0): The isolated yield was 120 mg (67%), M_n = 48.4 kDa, M_w = 96.6 kDa, PDI = 2.0. ^{1}H NMR (600 MHz, $C_2D_2Cl_4$, δ): 8.93 (br, 2H), 7.01 (br, 4H), 4.09 (br, 4H), 1.97 (br, 2H), 1.25 (64H), 0.87 (br, 12H). Anal. calcd. for $C_{56}H_{88}N_2O_2S_2$: C, 75.96; H, 10.02; N, 3.16; O, 3.61; S, 7.24; found: C, 75.75; H, 10.03; N, 3.12; O, 3.31; S, 7.25.

Synthesis of Poly(2,5-bis(2-octyldodecyl)-3,6-di(thiophen-2-yl)pyrrolo[3,4-c]pyrrole-1,4-dione)-alt-1-(2-thienyl)vinyl-5,5'-diyl) (DPP-TVT-1): The isolated

yield was 110 mg (61%), M_n = 49.2 kDa, M_w = 93.5 kDa, PDI = 1.9. ^{1}H NMR (600 MHz, $C_2D_2Cl_4$, δ): 8.93 (br, 2H), 7.01 (br, 6H), 4.09 (br, 4H), 1.97 (br, 2H), 1.25 (64H), 0.87 (br, 12H). Anal. calcd. for $C_{60}H_{90}N_2O_2S_3$: C, 74.48; H, 9.38; N, 2.90; O, 3.31; S, 9.94; found: C, 74.34; H, 9.18; N, 2.71; O, 3.44; S, 9.70.

Synthesis of Poly(2,5-bis(2-octyldodecyl)-3,6-di(thiophen-2-yl)pyrrolo[3,4-c] pyrrole-1,4-dione)-alt-1-(2-ditihenyl)vinyl-5,5′-diyl) (DPP-TVT-2): The isolated yield was 80 mg (56%), M_n = 23.5 kDa, M_w = 68.3 kDa, PDI = 2.9. ^{1}H NMR (600 MHz, $C_2D_2Cl_4$, δ): 8.93 (br, 2H), 7.01 (br, 8H), 4.09 (br, 4H), 1.97 (br, 2H), 1.25 (64H), 0.87 (br, 12H). Anal. calcd. for $C_{64}H_{92}N_2O_2S_4$: C, 73.23; H, 8.83; N, 2.67; O, 3.05; S, 12.22; found: C, 73.16; H, 8.77; N, 2.89; O, 3.03; S, 12.57.

Supporting Information

Supporting Information is available from the Wiley Online Library or from the author.

Acknowledgements

D.Y. and B.N.-Y. contributed equally to this work. This research was supported by the Basic Science Research Program through the National Research Foundation of Korea (NRF) funded by the Korean Ministry of Science, ICT, and Future Planning (Grant No.: 2013R1A1A1A05004475, 2010–0019408, BK21 Plus (10Z20130011057)). This research was also supported by the International Cooperation of the Korea Institute of Energy Technology Evaluation and Planning (KETEP) grant funded by the Korean Ministry of Knowledge Economy (No. 20123010010140), the Center for Advanced Soft-Electronics funded by the Ministry of Science, ICT, and Future Planning as Global Frontier Project (2013M3A6A5073183), and by the Dongguk University Research Fund of 2013. Experiments at the PLS-II 9A U-SAXS beamline were supported, in part, by MEST and POSTECH. Scheme 1 was revised on January 27, 2015.

Received: October 9, 2014
Revised: November 12, 2014
Published online: December 8, 2014

[1] a) A. R. Murphy, J. M. J. Fréchet, *Chem. Rev.* **2007**, *107*, 1066; b) P. M. Beaujuge, J. M. J. Fréchet, *J. Am. Chem. Soc.* **2011**, *133*, 20009; c) H. Huang, N. Zhou, R. P. Ortiz, Z. Chen, S. Loser, S. Zhang, X. Guo, J. Casado, J. T. López Navarrete, X. Yu, A. Facchetti, T. J. Marks, *Adv. Funct. Mater.* **2014**, *24*, 2782; d) J. Kim, B. Lim, K.-J. Baeg, Y.-Y. Noh, D. Khim, H.-G. Jeong, J.-M. Yun, D.-Y. Kim, *Chem. Mater.* **2011**, *23*, 4663; e) D. Boudinet, M. Benwadih, S. Altazin, J.-M. Verilhac, E. De Vito, C. Serbutoviez, G. Horowitz, A. Facchetti, *J. Am. Chem. Soc.* **2011**, *133*, 9968; f) I. McCulloch, M. Heeney, M. L. Chabinyc, D. DeLongchamp, R. J. Kline, M. Cölle, W. Duffy, D. Fischer, D. Gundlach, B. Hamadani, R. Hamilton, L. Richter, A. Salleo, M. Shkunov, D. Sparrowe, S. Tierney, W. Zhang, *Adv. Mater.* **2009**, *21*, 1091; g) J. Zaumseil, H. Sirringhaus, *Chem. Rev.* **2007**, *107*, 1296; h) P.-L. T. Boudreault, A. Najari, M. Leclerc, *Chem. Mater.* **2010**, *23*, 456; i) M. S. Chen, O. P. Lee, J. R. Niskala, A. T. Yiu, C. J. Tassone, K. Schmidt, P. M. Beaujuge, S. S. Onishi, M. F. Toney, A. Zettl, J. M. J. Fréchet, *J. Am. Chem. Soc.* **2013**, *135*, 19229; j) G. Kim, S.-J. Kang, G. K. Dutta, Y.-K. Han, T. J. Shin, Y.-Y. Noh, C. Yang, *J. Am. Chem. Soc.* **2014**; k) J. Lee, A. R. Han, J. Kim, Y. Kim, J. H. Oh, C. Yang, *J. Am. Chem. Soc.* **2012**, *134*, 20713; l) J. Lee, A. R. Han, H. Yu, T. J. Shin, C. Yang, J. H. Oh, *J. Am. Chem. Soc.* **2013**, *135*, 9540; m) W. Li, K. H. Hendriks, A. Furlan, W. S. C. Roelofs, M. M. Wienk, R. A. J. Janssen, *J. Am. Chem. Soc.* **2013**, *135*, 18942; n) R. J. Kline, M. D. McGehee, E. N. Kadnikova, J. Liu, J. M. J. Fréchet, M. F. Toney, *Macromolecules* **2005**, *38*, 3312; o) L.-L. Chua, J. Zaumseil, J.-F. Chang, E. C. W. Ou, P. K. H. Ho, H. Sirringhaus, R. H. Friend, *Nature* **2005**, *434*, 194.

[2] a) W. Hong, B. Sun, C. Guo, J. Yuen, Y. Li, S. Lu, C. Huang, A. Facchetti, *Chem. Commun.* **2013**, *49*, 484; b) H. Chen, Y. Guo, G. Yu, Y. Zhao, J. Zhang, D. Gao, H. Liu, Y. Liu, *Adv. Mater.* **2012**, *24*, 4618; c) J. Li, Y. Zhao, H. S. Tan, Y. Guo, C. A. Di, G. Yu, Y. Liu, M. Lin, S. H. Lim, Y. Zhou, H. Su, B. S. Ong, *Sci. Report* **2012**, *2*, 754; d) J. Kim, K.-J. Baeg, D. Khim, D. T. James, J.-S. Kim, B. Lim, J.-M. Yun, H.-G. Jeong, P. S. K. Amegadze, Y.-Y. Noh, D.-Y. Kim, *Chem. Mater.* **2013**, *25*, 1572.

[3] a) S. Cho, J. Lee, M. Tong, J. H. Seo, C. Yang, *Adv. Funct. Mater.* **2011**, *21*, 1910; b) J. Lee, A. R. Han, J. Hong, J. H. Seo, J. H. Oh, C. Yang, *Adv. Funct. Mater.* **2012**, *22*, 4128; c) Z. Chen, M. J. Lee, R. Shahid Ashraf, Y. Gu, S. Albert-Seifried, M. Meedom Nielsen, B. Schroeder, T. D. Anthopoulos, M. Heeney, I. McCulloch, H. Sirringhaus, *Adv. Mater.* **2012**, *24*, 647; d) C. B. Nielsen, M. Turbiez, I. McCulloch, *Adv. Mater.* **2013**, *25*, 1859; e) M. S. Chen, J. R. Niskala, D. A. Unruh, C. K. Chu, O. P. Lee, J. M. J. Fréchet, *Chem. Mater.* **2013**, *25*, 4088; f) X. Guo, N. Zhou, S. J. Lou, J. W. Hennek, R. Ponce Ortiz, M. R. Butler, P.-L. T. Boudreault, J. Strzalka, P.-O. Morin, M. Leclerc, J. T. López Navarrete, M. A. Ratner, L. X. Chen, R. P. H. Chang, A. Facchetti, T. J. Marks, *J. Am. Chem. Soc.* **2012**, *134*, 18427; g) T. Lei, J.-H. Dou, Z.-J. Ma, C.-H. Yao, C.-J. Liu, J.-Y. Wang, J. Pei, *J. Am. Chem. Soc.* **2012**, *134*, 20025; h) Y. Li, P. Sonar, S. P. Singh, M. S. Soh, M. van Meurs, J. Tan, *J. Am. Chem. Soc.* **2011**, *133*, 2198; i) X. Guo, S. R. Puniredd, B. He, T. Marszalek, M. Baumgarten, W. Pisula, K. Müllen, *Chem. Mater.* **2014**, *26*, 3595.

[4] S. Holliday, J. E. Donaghey, I. McCulloch, *Chem. Mater.* **2014**, *26*, 647.

[5] a) H. Chen, Y. Guo, Z. Mao, G. Yu, J. Huang, Y. Zhao, Y. Liu, *Chem. Mater.* **2013**, *25*, 3589; b) I. Kang, T. K. An, J.-a. Hong, H.-J. Yun, R. Kim, D. S. Chung, C. E. Park, Y.-H. Kim, S.-K. Kwon, *Adv. Mater.* **2013**, *25*, 524.

[6] J. R. Matthews, W. Niu, A. Tandia, A. L. Wallace, J. Hu, W.-Y. Lee, G. Giri, S. C. B. Mannsfeld, Y. Xie, S. Cai, H. H. Fong, Z. Bao, M. He, *Chem. Mater.* **2013**, *25*, 782.

[7] E. Wang, Z. Ma, Z. Zhang, K. Vandewal, P. Henriksson, O. Inganäs, F. Zhang, M. R. Andersson, *J. Am. Chem. Soc.* **2011**, *133*, 14244.

[8] a) G. K. Dutta, A. R. Han, J. Lee, Y. Kim, J. H. Oh, C. Yang, *Adv. Funct. Mater.* **2013**, *23*, 5317; b) J. C. Bijleveld, R. A. M. Verstrijden, M. M. Wienk, R. A. J. Janssen, *J. Mater. Chem.* **2011**, *21*, 9224; c) T. Lei, Y. Cao, Y. Fan, C.-J. Liu, S.-C. Yuan, J. Pei, *J. Am. Chem. Soc.* **2011**, *133*, 6099; d) Z. Ma, E. Wang, M. E. Jarvid, P. Henriksson, O. Inganas, F. Zhang, M. R. Andersson, *J. Mater. Chem.* **2012**, *22*, 2306.

[9] a) J. C. Bijleveld, M. Shahid, J. Gilot, M. M. Wienk, R. A. J. Janssen, *Adv. Funct. Mater.* **2009**, *19*, 3262; b) T. Lei, Y. Cao, X. Zhou, Y. Peng, J. Bian, J. Pei, *Chem. Mater.* **2012**, *24*, 1762; c) H. Zhou, L. Yang, W. You, *Macromolecules* **2012**, *45*, 607.

[10] a) H. Sirringhaus, *Adv. Mater.* **2005**, *17*, 2411; b) D. Natali, M. Caironi, *Adv. Mater.* **2012**, *24*, 1357.

[11] Y. Xu, T. Minari, K. Tsukagoshi, J. A. Chroboczek, G. Ghibaudo, *J. Appl. Phys.* **2010**, *107*, 114507.

[12] a) I. McCulloch, M. Heeney, C. Bailey, K. Genevicius, I. MacDonald, M. Shkunov, D. Sparrowe, S. Tierney, R. Wagner, W. Zhang, M. L. Chabinyc, R. J. Kline, M. D. McGehee, M. F. Toney, *Nat. Mater.* **2006**, *5*, 328; b) H. Sirringhaus, P. J. Brown, R. H. Friend, M. M. Nielsen, K. Bechgaard, B. M. W. Langeveld-Voss, A. J. H. Spiering, R. A. J. Janssen, E. W. Meijer, P. Herwig, D. M. de Leeuw, *Nature* **1999**, *401*, 685.

[13] A. M. Hindeleh, R. Hosemann, *J. Phys. C: Solid State Phys.* **1988**, *21*, 4155.

[14] a) F. Ç. Cebeci, H. Geyik, E. Sezer, A. Sezai Sarac, *J. Electroanal. Chem.* **2007**, *610*, 113; b) A. Bilge, A. Zen, M. Forster, H. Li, F. Galbrecht, B. S. Nehls, T. Farrell, D. Neher, U. Scherf, *J. Mater. Chem.* **2006**, *16*, 3177.

[15] R. C. Hynes, Y. Le Page, *J. Appl. Cryst.* **1991**, *24*, 352.